as used by Farquhar.[9] The required periodic solution is substituted in Eqs. (8) to give

$$\begin{Bmatrix} \xi_0 \\ \eta_0 \end{Bmatrix} = -\begin{Bmatrix} \Omega_*^2 + 2\Omega_*^2 - U_{yy}^0 \\ \Omega_*^2 + 2\Omega_*^2 - U_{yy}^0 \end{Bmatrix} \tag{10}$$

Since $U_{xx}^0 \neq U_{yy}^0$, the trajectory will be an ellipse centered on the L_2 point. The required radiation pressure acceleration may be obtained as

$$a_0 = \cos^{-3}\gamma \left[\frac{\Omega_*^4 - \Omega_*^2(U_{xx}^0 + U_{yy}^0 + 4) + U_{xx}^0 U_{yy}^0}{U_{yy}^0 - 2\Omega_* - \Omega_*^2} \right] \xi_0 \tag{11}$$

The uncoupled out-of-plane motion defined by Eq. (8c) may now be solved by Laplace transforms to give a general solution of the form

$$\begin{aligned} \zeta(t) = \zeta_0 \cos(\omega t) + \left(\frac{d\zeta}{dt}\right)_0 (U_{zz}^0)^{-1/2} \sin(\omega t) \\ + a_0 \cos^2\gamma \sin\gamma (U_{zz}^0)^{-1}[U(t) - \cos(\omega t)] \end{aligned} \tag{12}$$

where $U(t)$ is the unit step function and $\omega = (U_{zz}^0)^{1/2}$. Choosing $(d\zeta/dt)_0 = 0$, the solution can be more conveniently expressed as

$$\begin{aligned} \zeta(t) = U(t) a_0 \cos^2\gamma \sin\gamma (U_{zz}^0)^{-1} + \cos(\omega t) \\ \times [\zeta_0 - a_0 \cos^2\gamma \sin\gamma (U_{zz}^0)^{-1}] \end{aligned} \tag{13}$$

It can be seen from this form of the solution that once the sail is pitched from $\gamma = 0$ at $t = 0$ the motion is of the form of periodic oscillations at an out-of-plane distance $a_0 \cos^2\gamma \sin\gamma (U_{zz}^0)^{-1}$. By choosing the initial out-of-plane distance $\zeta_0 = a_0 \cos^2\gamma \sin\gamma (U_{zz}^0)^{-1}$, the sail remains at this fixed distance. The ζ component of the radiation pressure acceleration, and so the out-of-plane distance, may be maximized by an optimal choice of sail pitch angle γ^*, viz.,

$$\frac{d}{d\gamma} a_0 \cos^2\gamma \sin\gamma = 0 \Rightarrow \gamma^* = \tan^{-1}(2^{-1/2}), \quad (\simeq 35°.264) \tag{14}$$

Using this optimal pitch angle, the sail may execute an out-of-plane elliptical trajectory centered at the L_2 point.

The sail may be placed on such a trajectory by inserting it into a suitable elliptic path about the L_2 point. Once the sail is pitched to an angle γ^*, the out-of-plane oscillations may be damped in a time optimal manner. The optimal damping of such a system has been considered by Bryson and Ho.[10]

Applications

A moderate performance solar sail on such an out-of-plane ellipse could be used to demonstrate the use of the L_2 point for lunar far-side communications. At an out-of-plane distance of 3.5×10^3 km, both the lunar far-side and the equatorial regions of the Earth would be visible, requiring a sail acceleration on the order of 0.2 mms^{-2}. The trajectory itself would be a narrow ellipse with semimajor and minor axes of 1.105×10^4 km ($\eta_0 = 2.876 \times 10^{-2}$) and 5.655×10^2 km ($\xi_0 = 1.471 \times 10^{-3}$) and a period of 29.53 days (synodic lunar month); see Fig. 2. Since trajectories in the neighborhood of the lunar L_2 point are naturally unstable, active control will be required to ensure damping of the divergent modes. Also, the neglected nonlinear terms in Eqs. (8) will perturb the sail from its nominal elliptic trajectory. Even allowing for the idealizations of the dynamical model though, it is proposed that such a trajectory could be flown with the solar sails now being designed for the solar sail Moon race.

Acknowledgment

This work was carried out with the support of a Royal Society of Edinburgh Robert Cormack Fellowship.

References

[1]Friedman, L., et al., "Solar Sailing—The Concept Made Realistic," AIAA Paper 78-82, Jan. 1978.

[2]Sauer, C. G., "Optimum Solar Sail Interplanetary Trajectories," AIAA Paper 76-792, Aug. 1976.

[3]Forward, R. L., "The Statite: A Non-Orbiting Spacecraft," AIAA Paper 89-2546, July 1989.

[4]McInnes, C. R., and Simmons, J. F. L., "Halo Orbits for Solar Sails—Dynamics and Applications," *ESA Journal,* Vol. 13, No. 3, 1989, pp. 229–234.

[5]McInnes, C. R., and Simmons, J. F. L., "Solar Sail Halo Orbits I: Heliocentric Case," *Journal of Spacecraft and Rockets*, Vol. 29, No. 4, 1992, pp. 466–471.

[6]McInnes, C. R., and Simmons, J. F. L., "Solar Sail Halo Orbits II: Geocentric Case," *Journal of Spacecraft and Rockets*, Vol. 29, No. 4, 1992, pp. 472–479.

[7]Perret, A., LaBombard, E., and Koryo, M., "The Solar Sail Race to the Moon," IAF Paper 89-539, Oct. 1989.

[8]Vonbun, F. O., "A Hummingbird for the L_2 Lunar Libration Point," NASA TN-D-4468, April 1968.

[9]Farquhar, R. W., "The Control and Use of Libration Point Satellites," NASA TR-R-346, Sept. 1970.

[10]Bryson, A. E., and Ho, Y.-C., *Applied Optimal Control,* Blaisdell, Waltham, MA, 1969, pp. 156–157.

Antoni K. Jakubowski
Associate Editor

Dynamic Response Spectra for an Aerospace Payload and its Attachments

Gina Lee-Glauser* and Goodarz Ahmadi†
Clarkson University, Potsdam, New York 13699

Nomenclature

$A(X)$ = cross-sectional area
a = nonuniformity constant
C_o = payload damping coefficient
G = shear modulus
K = geometry constant factor
L = total height of the payload
m_o = mass of the payload
m_s = mass of the secondary system
N = number of modes
q_n = modal amplitude
u = deflection of the payload relative to its base
$\ddot{u}_l$ = launch vehicle acceleration
X = distance from the base
x = dimensionless height
$z(t)$ = subsystem displacement relative to the payload
ζ_n = payload damping coefficient
ζ_s = secondary system damping coefficient
λ_n = payload eigenvalue
ρ_o = mass density per unit volume
ϕ_n = normal mode
ω_n = payload natural frequency
ω_s = secondary system natural frequency

Introduction

AN aerospace payload generally contains a number of highly sensitive and expensive subsystems such as satellite antennas, solar arrays, and other sensitive accessories. It

Received Aug. 16, 1991; revision received Oct. 25, 1991; accepted for publication Feb. 14, 1992.

*Graduate Student, Department of Mechanical and Aeronautical Engineering.

†Professor, Department of Mechanical and Aeronautical Engineering.

is, therefore, very crucial to guarantee structural and functional integrity of the payload in all stages of flight from the lift-off to deployment in space. In practice, the payload contains numerous delicate and expensive parts and attachments, therefore, protecting these sensitive subsystems is as important as the payload itself. A successful payload deployment depends on the functional integrity of its many sensitive subsystems.

In this study, the payload and one of its subsystems are treated as primary and secondary systems. The subsystem is modeled as a damped single-degree-of-freedom oscillator attached to a nonuniform shear beam payload model. Interactions between the secondary system and the primary payload structure are included in the analysis. A sinusoidal and the Space Transportation System mission 41 (STS-41) liftoff accelerations are used as the dynamic input of the launcher. The peak acceleration response of the payload and its subsystem under various conditions are evaluated and the results are presented as response spectra curves. Particular attention is given to the effects of mass ratio of the subsystem. The significance of the primary-secondary interactions and mass ratio for near-tuned conditions are also studied.

Formulation of the Shear Beam Structure Model

It is assumed that the payload structure may be modeled as an elastic nonuniform shear beam. The governing equations of motion of the shear beam structure subject to a launch vehicle interface acceleration $\ddot{u}_l$ is given by

$$\rho_o A(X)\frac{\partial^2 u(X,t)}{\partial t^2} + C_o A(X)\frac{\partial u(X,t)}{\partial t} - \frac{\partial}{\partial X}\left[KGA(X)\frac{\partial u(X,t)}{\partial X}\right]$$

$$= -\rho_o A(X)\ddot{u}_l(t) + F_s(t)\delta(X-H), \quad 0 \le X \le L \tag{1}$$

Here, $F_s(t)$ is the force exerted by the subsystem on the payload, and $\delta(X-H)$ is the Dirac delta function which indicates that the concentrated force is applied at the attachment point of the subsystem, $X = H$. The boundary conditions are

$$u(0,t) = 0, \qquad \frac{\partial u(L,t)}{\partial X} = 0 \tag{2}$$

The force $F_s(t)$ in Eq. (1) is given by

$$F_s(t) = m_s\,[2\zeta_s\omega_s\dot{z}(t) + \omega_s^2 z(t)] = -m_s[\ddot{z}(t) + \ddot{u}_l(t) + \ddot{u}(H,t)] \tag{3}$$

It is assumed that the cross-sectional area of the payload varies as

$$A = A_o e^{-2ax}, \qquad x = X/L, \qquad h = H/L \tag{4}$$

The normal modes of vibration of a simple nonuniform shear beam with no attachment subject to the boundary conditions given by Eq. (2) were described in Ref. 1. The general solution to Eq. (1) may be assumed to be given as

$$u(x,t) = \sum_{n=1}^{N} q_n(t)\phi_n(x) \tag{5}$$

where the modal amplitudes are determined by

$$\ddot{q}_n(t) + 2\zeta_n\omega_n\dot{q}_n(t) + \omega_n^2 q_n(t) = -\alpha_n\ddot{u}_l(t) + [2\zeta_s\omega_s\dot{z}(t) + \omega_s^2 z(t)]\,R_{s1}\phi_n(h) \tag{6}$$

where

$$\omega_n^2 = \frac{KG}{\rho_o L^2}(\lambda_n^2 + a^2), \qquad \zeta_n = \frac{C_o}{2\rho_o\omega_n}$$

A listing of the eigenvalues λ_n were provided in Ref. 1. The coefficients α_n and R_{s1} Eq. (6) are given by

$$\alpha_n = \beta_n\lambda_n/(\lambda_n^2 + a^2), \; R_{s1} = (1 - e^{-2a})/2a]\; R_s/R$$

$$\beta_n = \frac{2}{\sqrt{2 - \sin(2\lambda_n)/\lambda_n}} \tag{7}$$

Here, the mass ratios are defined as

$$R = m_o/m_p, \qquad R_s = m_s/m_p, \qquad m_p = m_o + m_s \tag{8}$$

The equation of motion of the subsystem in terms of the shear beam response at the attachment point is given as

$$\ddot{z}(t) + 2\zeta_s\omega_s\dot{z}(t) + \omega_s^2 z(t) = -\ddot{u}_l(t) - \sum_{n=1}^{N}\phi_n(h)\ddot{q}_n(t) \tag{9}$$

Equations (6) and (9) can now be solved for the payload modal amplitude and subsystem deflection. Additional details of the analysis are described in Ref. 2.

In the subsequent analysis, $f_1 = 4.6$ Hz ($\omega_1 = 9.2\pi$ rad/s), $\zeta_n = 0.01$, and $a = 0.1$ are used.

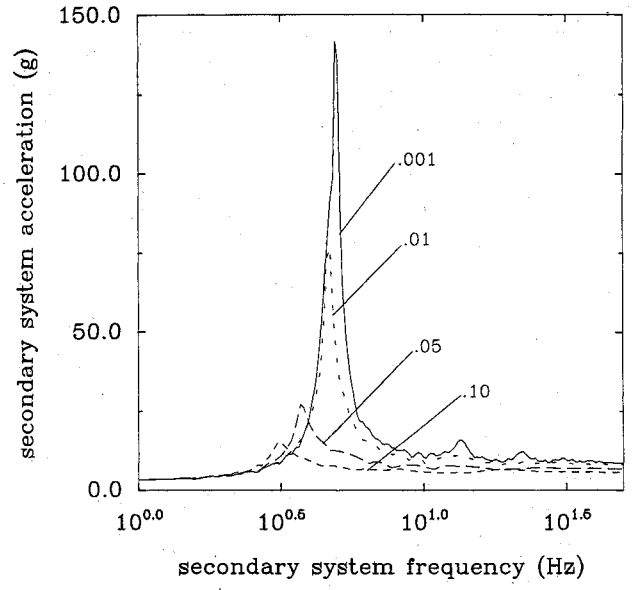

Fig. 1 Peak acceleration responses of subsystem for various mass ratios under the sinusoidal excitation for $f_1 = 4.6$ Hz.

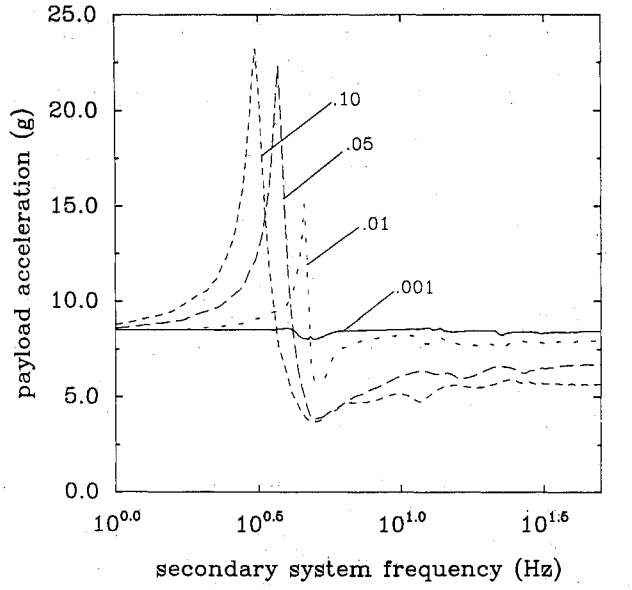

Fig. 2 Payload peak acceleration responses for various mass ratios under the sinusoidal excitation for $f_1 = 4.6$ Hz.

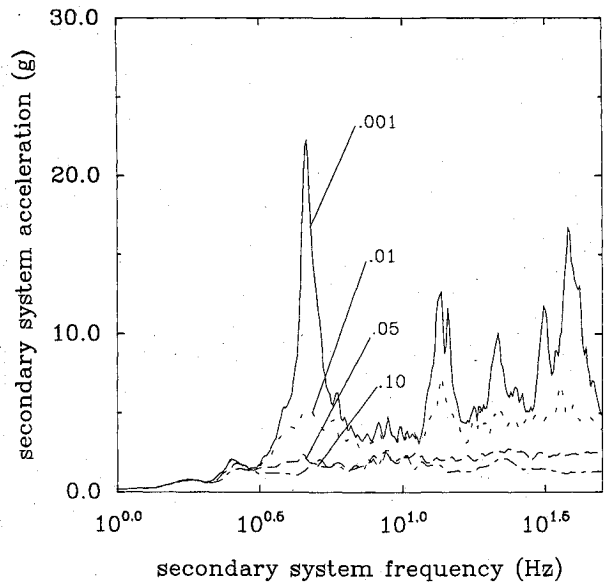

Fig. 3 Peak acceleration responses of subsystem for various mass ratios for the STS-41 *Z* acceleration for $f_1 = 4.6$ Hz.

Sinusoidal Excitation

A typical launch vehicle natural frequency of 5 Hz ($T_l = 0.2$ s) is used as the sinusoidal excitation frequency. The launch vehicle acceleration at the payload support then is given by

$$\ddot{u}_l = 1.56g + 0.5g \sin(2\pi t/T_l) \tag{10}$$

The offset of 1.56*g* is added to account for the solid rocket booster ignition.

Figure 1 shows the subsystem response spectra for the payload fundamental natural frequency of 4.6 Hz. It is observed that the amplitude of the resonance peak is sharply reduced as the mass ratio increases. In addition, the resonance frequency appears to be somewhat reducing as R_s increases. Figure 2 shows the payload peak acceleration responses for various subsystem frequencies. At the tuning frequency of $f_s \simeq 5.0$ Hz, the secondary system behaves as a dynamic-tuned mass energy absorber and the payload spectral amplitudes are reduced by about 40%. For larger f_s, the payload vibration amplitude is generally reduced. It is also observed that larger accelerations are experienced by the payload as mass ratio increases.

Figures 1 and 2 show that the tuning frequency shifts with an increase in mass ratio. The direction of the frequency shift is a function of the ratio of the fundamental natural frequency of the payload to the driving frequency. This trend of variation is consistent with the analytical results described in Ref. 2.

STS-41 ACIP Liftoff Acceleration

In this section, the lift-off accelerations of the STS-41 Aerodynamic Coefficient Instrumentation Package (ACIP) in the *Z* direction is used. Figure 3 shows the subsystem response spectra for different mass ratios. Additional peaks due to to the higher modes of vibration of the payload are also clearly observed in this figure. The response amplitude of the fifth mode is about 75% of that of the first mode. This is because the *Z* acceleration contains considerable amount of energy at high frequencies ($f_s \geq 30$ Hz). As the mass ratio increases, the resonance peaks for higher modes decrease rather sharply. Additional results concerning effects of damping and STS-41 X acceleration are described in Ref. 2.

Conclusions

The presented results show that a light subsystem may experience much larger loading than its payload. Therefore, structural safety of the subsystem for the liftoff condition must be carefully analyzed. The subsystem mass ratio has a significant effect on its peak responses for both sinusoidal excitation and STS-41 liftoff ACIP accelerations. The primary-secondary interactions, generally, reduce the peak responses of the subsystem. The amount of reduction increases significantly as the mass ratio increases. The tuning frequency shifts with an increase in mass ratio. The direction of the tuning frequency shift is a function of the ratio of the fundamental natural frequency of the payload to the driving frequency.

Acknowledgments

This work was supported by the National Science Foundation Grant EID-9017559. Many thanks are given to D. Hamilton and J. Dagen from NASA Johnson Space Center and J. Brose and D. Hackler from Lockheed, Software Development Section, for many helpful discussions and supplying the STS-41 flight data.

References

[1]Su, L., and Ahmadi, G., "Earthquake Response of Linear Continuous Structures by the Method of Evolutionary Spectra," *Engineering Structures*, Vol. 10, 1988, pp. 47–56.

[2]Lee-Glauser, G., and Ahmadi, G., "Dynamic Response Spectra for an Aerospace Payload and Its Attachments," Clarkson Univ., Rept. MAE-232, Potsdam, NY, May 1991.

Earl A. Thornton
Associate Editor

Shaped Discharge Ports for Draining Liquids

K. Ramamurthi* and T. John Tharakan†
Liquid Propulsion Systems Centre, Valiamala, Trivandrum 695 547, India

Introduction

THE formation of a vortex core during the draining of liquids from tanks not only leads to a reduced outflow but also causes air to be ingested in the discharge. Explicit predictions for the height of the air vortex formed is not possible in free draining situations. The Rankine compound vortex model, which is a combination of free vortex with a forced vortex inside, cannot take into account the axial velocity due to the efflux and the dissipation of vorticity from the core. Dergarabedian[1] has proposed a theoretical model that considers the influence of the efflux on the tangential velocity. However, the analysis is for a liquid that extends to infinity in the radial direction and gives only a qualitative insight into the phenomenon. To evolve the scaling laws for air-vortex formation and hence adopt a scheme to arrest the formation, a series of well-planned experiments were conducted in cylindrical containers with different sizes of drain ports. The results suggest that the incidence of air-vortex formation while draining liquids from tanks can be reduced by suitable shaping of the drain ports.

Rotational motion in the liquid can assist in the formation of vortex. The scaling laws for vortex formation and the effectiveness of shaped ports in suppressing air vortex are studied separately for conditions when 1) the liquid column is initially quiescent and 2) rotational currents are present in the liquid column.

Received April 8, 1992; revision received June 25, 1992; accepted for publication June 29, 1992.

*Head, Propulsion Research and Studies Group.

†Engineer, Propulsion Research and Studies Group.